Design and characterization of a device to quantify the magnetic drug targeting efficiency of magnetic nanoparticles in a tube flow phantom by magnetic particle spectroscopy

Patricia Radon*, Norbert Löwa, Dirk Gutkelch, Frank Wiekhorst

Physikalisch-Technische Bundesanstalt, Abbestrasse 2-12, 10587 Berlin, Germany

ABSTRACT

The aim of magnetic drug targeting (MDT) is to transfer a therapeutic drug coupled to magnetic nanoparticles (MNP) to desired disease locations (e.g. tumor region) with the help of magnetic field gradients. To transfer the MDT approach into clinical practice a number of important issues remain to be solved. We developed and characterized an in-vitro flow phantom to provide a defined and reproducible MDT environment. The tube system of the flow phantom is directed through the detection coil of a magnetic particle spectroscopy (MPS) device to determine the targeting efficiency. MPS offers an excellent temporal resolution of seconds and an outstanding specific sensitivity of some nanograms of iron. In the flow phantom different MNP types, magnet geometries and tube materials can be employed to vary physical parameters like diameter, flow rate, magnetic targeting gradient, and MNP properties.

1. Introduction

Magnetic nanoparticles (MNP) are exploited for novel biomedical diagnostic and therapeutic approaches. One promising approach in cancer therapy is magnetic drug targeting (MDT). Here, the MNP serve as a transporter of a chemotherapeutic agent guided through the blood vessels of the body and finally accumulated at a target region by magnetic fields. This should effectively reduce unwanted side effects associated with conventional systemic chemotherapy. Preclinical studies in animal models [1–3] and a first clinical human trial [4] showed that to transfer MDT into clinical practice still some challenges have to be mastered [5]. Only few MNP systems have been approved for venous or arterial administration in humans so far. Therefore, the development of sophisticated MNP for MDT is still challenging, requiring dedicated MNP properties meeting various clinical needs [5]. Too large particle sizes or the aggregation of MNP could clog blood vessels leading to fatal embolism. On the other hand, MNP must be large enough to transport the required amount of drug and have a sufficiently large magnetic moment to deploy an acceptable magnetic force in the external magnetic field (gradient) [6]. The magnetic force decreases with increasing distance from the magnet, so that MDT is currently only applicable for target regions close to the body surface [7].

To assess the behavior of MNP in MDT applications under defined physiological and physical parameters we developed and constructed an in-vitro flow phantom. The flow phantom consists of a closed tube system mimicking a blood circuit. MNP suspended in a medium such as water or blood are circulated through the tube system by an integrated pump. In the retention area a targeting magnet can be positioned at a defined distance to the tube system to enrich the MNP by the magnetic field gradient. The targeting efficiency is determined by magnetic particle spectroscopy (MPS) using the non-linear dynamic magnetic susceptibility of MNP for their sensitive and specific quantitative detection. First successful measurements using this technique in a very simple MDT setup already demonstrated the excellent sensitivity in MNP detection in the nanogram range [8]. In our extended flow phantom we implemented the online quantification of the MNP retention during the magnetic targeting process by conducting the circulating MNP through the detection coil of the MPS device.

2. Materials and methods

The flow phantom setup is composed of the magnet positioning unit, the tubing flow system with peristaltic pump and the MPS device for quantification of MNP. As shown in Fig. 1(left) the peristaltic pump circulates the MNP suspended in a medium through the closed polymer tube system. The tube system consists of the pump segment, targeting segment and flow cell segment with in and out flow. At the targeting
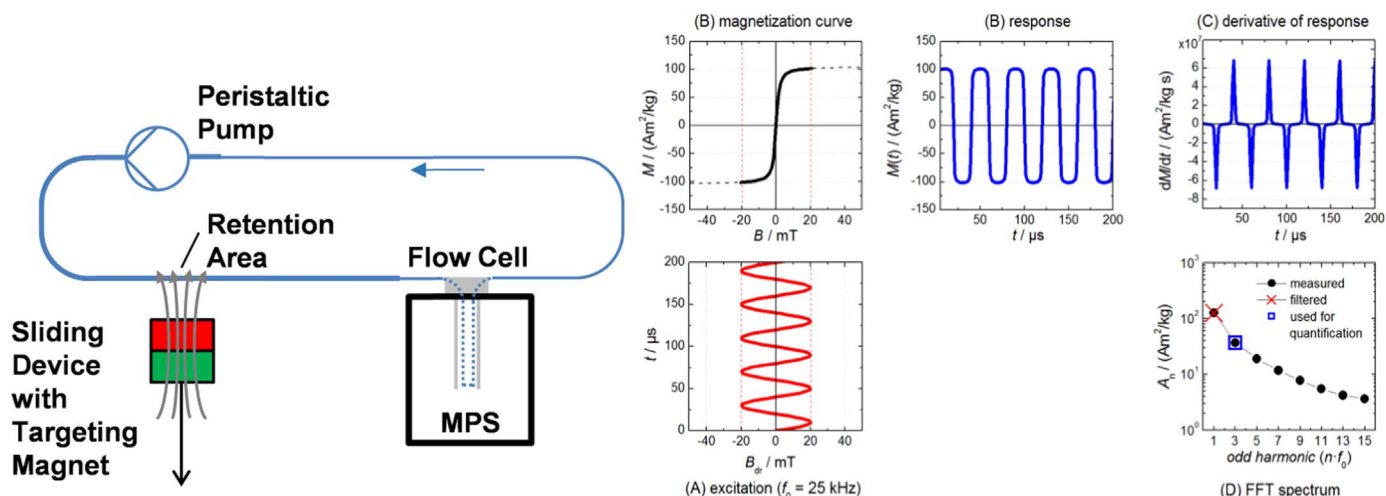
Fig. 1. Left: Setup of the flow phantom. The peristaltic pump circulates the MNP suspension through the closed polymer tube system. At the retention area a neodymium targeting magnet is located to accumulate MNP. To quantify the targeting efficiency a flow cell is used to direct the tube through the detection coil of the MPS-device. Right: Principle of MPS. The MNP are exposed to a sinusoidal oscillating magnetic excitation field (A) at frequency f_0=25 kHz and amplitude B_{ex}=25 mT. The non-linear magnetization of the MNP (B) leads to an oscillating response that also contains higher frequencies (C) of f_0. The derivative of the response (D) is then detected inductively by a detection coil. After high-pass filtering to suppress components at frequency f_0 the response is amplified and recorded. By Fourier transformation the MPS amplitude spectrum of odd harmonics A_n n=3, 5, 7, … is obtained (E).

segment the targeting magnet can be precisely positioned by a sliding device. For MNP quantification the flow cell segment is inserted into the detection coil of our MPS device.

2.1. Magnetic particle spectroscopy device for MNP quantification

Originally, MPS was developed to assess the capability of MNP to be used as tracer in the novel imaging modality magnetic particle imaging [9]. MPS is based on the detection of the non-linear dynamic magnetic susceptibility of MNP exposed to an oscillating excitation field. Fig. 1 (right) schematically shows the basic principle of MPS. The MNP are excited by a sinusoidal oscillating magnetic field at frequency f_0 and amplitude B_{ex}. Due to the non-linearity of the MNP magnetization curve $M(H)$ the MNP response $M(t)$ exhibits components at odd harmonics. The derivative of the response is detected as an induction voltage $U(t) \sim dB/dt$ by a pickup coil and first high-pass filtered to suppress the strong excitation component f_0, then amplified and recorded. Finally, a Fourier transformation is used to obtain a MPS amplitude spectrum A_n composed of odd multiples (due to the symmetry of the magnetization curve) of f_0. Excitation fields and the MPS amplitude spectra (in units of A m^2) of the device are absolutely calibrated using a traceable coil. In most cases, the third harmonic A_3 is employed for quantification, whereas the ratio between fifth and third harmonic A_5/A_3 (in percent) is used to characterize the shape of the MPS spectrum of a particular MNP system.

We used a commercial MPS device (MPS-3, Bruker BioSpin) operating at a fixed excitation frequency f_0=25 kHz and variable excitation field amplitudes B_{ex} between 0.05 mT and 25 mT [10]. At the highest excitation field B_{ex}=25 mT the spectrometer exhibits the highest sensitivity and can detect moments down to $5 \cdot 10^{-12}$ A m^2 [11]. The MPS amplitudes are linearly related to the MNP amount (or iron amount which often can be more precisely determined for MNP) which is exploited for quantification of MNP as described in Section 3.2. Furthermore, the device is capable to detect moments over more than 6 decades ($> 10^{-6}$ A m^2). In normal operation (batch mode) a sample volume of usually 30 μL is filled into a PCR cup and placed in the pickup coil of the MPS system using a specifically designed sample holder.

2.2. Tubing flow system

The MNP suspension under investigation is pumped by a peristaltic pump (IPC-N 4, Ismatec, Germany) through the tube system. The pump is equipped with a special Tygon 2-stopper tube of 1.4 mm diameter which allows adjusting a flow rate between 27 μL/min and 2.7 mL/min. We used a fixed flow rate of 350 μL/min in accordance with other in-vitro targeting setups [12–15]. In contrast, the targeting segment can be freely chosen to be able to simulate physical and physiological conditions (e.g. shape, diameter, material). In this work the targeting segment consists of the same tube material as used for the peristaltic pump.

To continuously quantify the accumulated MNP amount the tube system is directed through the pickup coil of the MPS device (flow cell tube). As standard our commercial MPS device is not designed for continuous flow measurements, thus we developed a dedicated MPS flow cell [16]. This flow cell was produced by generative manufacturing and consists of a hose guide of non-magnetic material (E-Shell 600 of EnvisionTEC GmbH, Germany) capable to house and to precisely guide and position the tube into the pickup coil. We employed fluorinated ethylene propylene (FEP) tube with 0.8 mm diameter and 2.5 windings to direct the flow volume in the sensitive area of the MPS detection coil. In Section 3.1 the influence of the different tube materials of the quantified iron amount is investigated.

2.3. Targeting magnet positioning unit

A sliding device is used to precisely position a conventional permanent magnet (neodymium-iron-boron alloy with an edge length of 10 ± 0.1 mm, Webcraft GmbH, Switzerland) at the retention area of the tube system with an accuracy of 0.4 mm. The magnetic force acting on the MNP and thereby the targeting efficiency is essentially determined by the magnetic field of the targeting magnet. With increasing distance to the magnet's surface the magnetic field gradient is strongly decreasing. Using a hall probe we estimated a gradient of about 83 T/m directly at the surface of the magnet and about 80 T/m at a distance of 1 mm from the magnet, corresponding to the wall thickness of the tube used in the targeting segment. Already at a distance of 4 mm the gradient dropped to about 40 T/m.

2.4. Magnetic nanoparticles for MDT

To characterize the MDT capability of our flow phantom setup three commercially available MNP types were used: the MRI liver contrast agent Resovist (Bayer Healthcare, Germany), Feraheme (AMAG Pharmaceuticals Inc.) which is used for treatment of iron deficiency

Table 1

Structural and magnetic MNP properties of FluidMAG-D, Resovist and Feraheme: Hydrodynamic diameter d_{hyd} obtained by DLS, saturation magnetization M_S, effective magnetic diameter d_v, distribution σ and magnetic moment μ_m from DC susceptometry.

MNP	d_{hyd} [nm]	M_S [A m^2/kg(Fe)]	d_v [nm]	σ	μ_m 10^{-20} [A m^2]	Core type	Coating
FluidMAG-D	190.2	106	8.7	0.3	13.9	Multi	Starch
Resovist	61.6	104	5.2[a]	0.47[a]	2.9	Single/multi	Carboxydextran
Feraheme	26.5	125	5.8	0.32	4.8	Single	Carbohydrate[a]

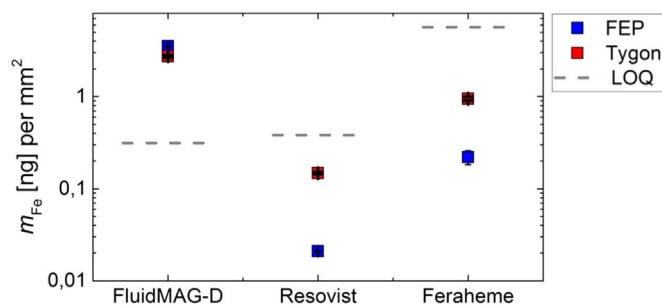[a] bimodal distribution (dv2=21.7 nm, σ2=0.29) as reported in [18].

Fig. 2. Adhesion of FluidMAG-D, Resovist, and Feraheme to Tygon and FEP tube material. The MPS signal of Feraheme and Resovist on FEP and Tygon was below the limit of quantification (LOQ), whereas FluidMAG-D showed a clear adhesion to the tube materials. Note, the uncertainty bars lie within the data symbol width.

anemia and the ferrofluid FluidMAG-D (Chemicell GmbH, Germany) employed for cell separation, MRI-diagnostics and MDT applications.

The targeting efficiency is essentially dominated by the magnetic and structural properties of the MNP [17]. The effective magnetic moment μ_m determines the magnetophoretic force

$$\mathbf{F}_M = (\mu_m \cdot \nabla)\mathbf{B}, \tag{1}$$

while the hydrodynamic diameter d_{hyd} affects the drag force:

$$\mathbf{F}_D = 6\pi\eta \frac{d_{hyd}}{2}(\mathbf{v}_{MNP} - \mathbf{v}_{medium}) \tag{2}$$

with the viscosity η and the velocity of the MNP ($\mathbf{v}_{MNP}$) and the medium ($\mathbf{v}_{medium}$). The magnetophoretic force $\mathbf{F}_M$ has to be greater than the drag force $\mathbf{F}_D$ in order to accumulate MNP by the targeting procedure. The structural and magnetic properties of the three MNP types are summarized in Table 1. The volume weighted hydrodynamic diameter d_{hyd} was determined by dynamic light scattering (DLS, Zetasizer NanoZS, Malvern Instruments, UK), the saturation magnetization M_S at room temperature, the effective magnetic diameter d_V with distribution σ and μ_m of the MNP were extracted from SQUID magnetometry (MPMS-XL, Quantum Design, San Diego, USA).

3. Results and discussion

The tube material employed for MPS flow measurements should not contain any magnetic impurities and exhibit minimum adhesion of MNP. Therefore, we tested different tube materials for magnetic impurities and checked the adhesion behavior of the MNP with the tube material. Subsequently, sensitivity and limit of quantification (LOQ) of MPS were determined for the three different MNP types. Finally, targeting experiments were carried out for the different MNP types to demonstrate the performance and reproducibility of the flow phantom.

3.1. Investigation magnetic impurities and MNP adhesion in tube materials

By MPS we measured the amplitude spectra (considering the third harmonic A_3 normalized to the inner surface of the tube sample under investigation) of five different tube materials: Silicone, fluorinated

ethylene propylene (FEP), Tygon, polytetrafluoroethylene (PTFE) and polyvinyl chloride (PVC). Only silicone exhibited detectable MPS signals due to magnetic impurities (A_3=3.3 µA m^2/m^2) while no impurities could be detected in the other materials (MPS moment A_3 below limit of quantification (LOQ) $1.7 \cdot 10^{-11}$ A m^2, see below).

Furthermore, the adhesion of MNP to tubing material might lead to losses of MNP in the tubing system distorting the MPS quantification. Therefore, we investigated the MNP adhesion to Tygon (targeting segment, pump tubing) and FEP (MPS flow cell). To this end an MNP suspension (at an iron concentration of 7.5 mmol/L) was filled into a tube section of 10 cm length. After 5 min the MNP suspension was rinsed out and flushed with ultra-pure water. Then, three pieces of defined length were cut out of the tube segment and separately measured by MPS. The mean MPS amplitude A_3 was normalized to the inner surface of the corresponding tube piece and by comparison to a reference sample of known iron amount we determined the specific adhered iron amount. The MPS signals of both investigated tube materials having been filled either with Feraheme or Resovist were below the limit of quantification (LOQ, see Section 3.2) indicating a negligible MNP adhesion. However, FluidMAG-D MNP showed significant adhesion to both tested materials (see Fig. 2), which was slightly higher for FEP (3.5 ng/mm^2) than for Tygon (2.7 ng/mm^2). Regarding the designed flow phantom comprising an overall tube length of 1.25 m we estimated a total adhesion of about 9 µg assuming homogeneous MNP adhesion. With a total iron amount of 400 µg in the MNP suspension typically applied in our targeting procedures this corresponds to about 2% MNP which are lost by adhesion to the tube inner surface of the tube in the case of FluidMAG-D. Thus, even for FluidMAG-D, adhesion of MNP to the tube inner surface only slightly influences the determination of the targeting efficiency.

3.2. Limit of detection, limit of quantification, MNP sensitivity A_3^* and influence of flow rate

The MPS device enables measurements at different excitation field amplitudes up to 25 mT which leads to significantly differing MPS signals of the investigated MNP types. As shown in Fig. 3 (left), the amplitude A_3 increases non-linearly with increasing excitation field B_{ex} exhibiting a characteristic behavior for each MNP type (samples containing 80 µg iron). At large B_{ex} values the tendency of saturation of A_3 becomes visible. The noise level of A_3 (determined from 150 empty MPS measurements) only displays a weak increase with excitation field as depicted by the grey dotted line in Fig. 3 (left). At this field value – still below the saturation field for all three MNP systems - the largest dynamic magnetization response is produced (covering the largest non-linearity regime of the magnetization curve). Therefore, the MPS measurements for quantification were performed at the highest excitation field B_{ex}=25 mT.

To determine the specific sensitivity A_3^*, which is the slope of the ratio between measured moment A_3 and corresponding iron amount, we measured for each MNP type a serial dilution at a given concentration (V=60 µL) as displayed in Fig. 3 (right). A highly linear A_3 dependency on iron amount is found with different slopes for each MNP type: A_3^*=9.8 A m^2/(kg Fe) for Resovist, A_3^*=7.3 A m^2/(kg Fe) for FluidMAG-D, and A_3^*=0.7 A m^2/(kg Fe) for Feraheme. This implies
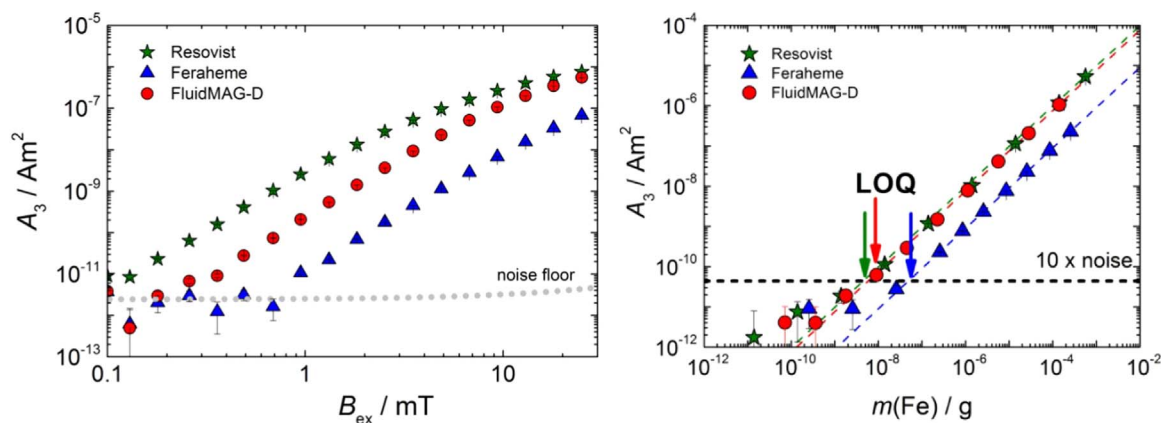
Fig. 3. Left: MPS amplitude A_3 as a function of MPS excitation field B_{ex} of for the three MNP types at an iron amount of about 80 µg. The largest moments A_3 are detected at the highest field value B_{ex}=25 mT. At low values B_{ex}, A_3 reaches the noise level (standard deviation determined from 150 empty measurements). Right: MPS amplitudes of the third harmonic A_3 as a function of nominal iron amount obtained by serial dilutions for Resovist, Feraheme, and FluidMAG-D. A_3 linearly increases with increasing iron amount, the slope is the MNP specific amplitude A_3^* used for quantification. The arrows denote the limit of quantification (LOQ) for the corresponding MNP type. The LOQ is given as the iron amount corresponding to an A_3 that is just ten times the noise level (1.7×10^{-11} A m^2 at B_{ex}=25 mT). (For interpretation of the references to color in this figure legend, the reader is referred to the web version of this article.)

that the sensitivity of MPS for Resovist is highest, closely followed by FluidMAG-D and one order of magnitude smaller for Feraheme. Then, by dividing the measured amplitude $A_{3,sample}$ of a sample by the sensitivity A_3^* the iron amount is obtained.

We followed the common definition used in analytical chemistry for the limit of quantification to be the iron amount corresponding to the A_3 moment equal to ten times the standard deviation of the blank (from MPS measurements of 20 empty sample tubes a value of $1.7 \cdot 10^{-11}$ A m^2 at B_{ex}=25 mT is obtained). As depicted in Fig. 3(right) by colored arrows LOQ=5 ng was found for Resovist, LOQ=8 ng for FluidMAG-D, and LOQ=60 ng for Feraheme. The values of A_3^* and LOQ for the three MNP types under investigation are summarized in Table 2.

Note, that the MPS signal variation of a continuous flow measurement (without changing the sample holder or flow cell) is lower than the signal variation of different empty vessels resulting in a lower noise level and consequently a lower LOQ of MPS flow measurements compared to conventional MPS measurements in batch mode [16].

In comparison to normal operation MPS measurements (batch mode, without flow) only little changes were found in the MPS amplitude A_3 when MNP are circulating through the MPS device [16]. At the flow rate of 350 µL/min, which we used in our targeting experiments, the signal amplitude A_3 of the three MNP types deviates only marginally (up to 3%) from A_3 measured in normal operation.

3.3. The targeting efficiency determined by MPS quantification

We define the targeting efficiency TE in the retention area as the ratio between the MNP amount m_{DT} accumulated by the magneto-phoretic force Eq. (1) (and diminished by the drag force Eq. (2) due to the flow) and the total MNP amount m_{total} present in the tube system

Table 2
Sensitivity A_3^*, limit of quantification LOQ and different targeting parameter (maximal accumulated MNP amount m_{max}, targeting efficiency TE, time constant τ and half-life period $t_{1/2}$) of FluidMAG-D, Resovist and Feraheme.

MNP system	A_3^*[Am^2/kg(Fe)]	LOQ [ng]	m_{max} [µg]	TE [%]	$t_{1/2}$ [min]
Resovist	9.8	5	19	4.8	47
FluidMAG-D	7.5	8	210	52.2	18
			208[a]	52.0[a]	52[a]
Feraheme	0.7	60	14	3.6	35

[a] FluidMAG-D suspended in stabilized blood.

$$TE = \frac{m_{DT}}{m_{total}}. \tag{3}$$

The total iron amount m_{total} employed in a targeting experiment is given by the product of total tube volume V_{total}, the iron concentration c(Fe) (in mol/L) and the molar mass of iron M_{Fe}

$$m_{total} = V_{total} \ c(Fe) \ M_{Fe}. \tag{4}$$

Here, we determined V_{total} experimentally from the weight difference between completely filled (with pure water) and empty tube system.

Off-site the retention area we assume a homogeneous MNP distribution and indirectly determine the accumulated iron amount m_{DT} from the iron amount m_{MPS} quantified in the flow cell by MPS given by

$$m_{MPS} = \frac{A_3}{A_3^*}, \tag{5}$$

so finally, m_{DT} is obtained as

$$m_{DT} = m_{total} - m_{MPS} \frac{V_{total}}{V_{fc}}, \tag{6}$$

where V_{fc} denotes the effective volume of the flow cell in the MPS detection coil. V_{fc} has been determined from the ratio between the measured MPS amplitude A_3 of MNP in the flow cell and a suspension of 30 µL of the same MNP measured in a PCR container.

As shown in Fig. 4(left), after pumping the MNP suspension in the tube system a transient behavior of the measured MPS signal during the first five circulations of the suspension is observed (period of one complete circulation lasts for about 3 min). After starting the pump A_3 decreases by about 3% (FluidMAG-D) and after 15 min nearly remains constant with an uncertainty of about 1%, so that only minor influence on the quantification procedure can be assumed. The transient behavior might be attributed to a temperature compensation effect, because the MNP suspension is filled into the tube system at room temperature and warms up to about 37 °C during the passage of the temperature-controlled MPS.

Therefore, we first circulated for 15 min the suspension without magnet and then started the actual targeting experiment by moving the magnet to the retention area (denoting the start point t_0) and keeping it there for a defined time interval (typical 120 min). During this period MPS measurements were repetitively performed at time intervals on a logarithmic time scale.

After removal of the targeting magnet the accumulated MNP at the retention area are partly released into the circulating suspension. For
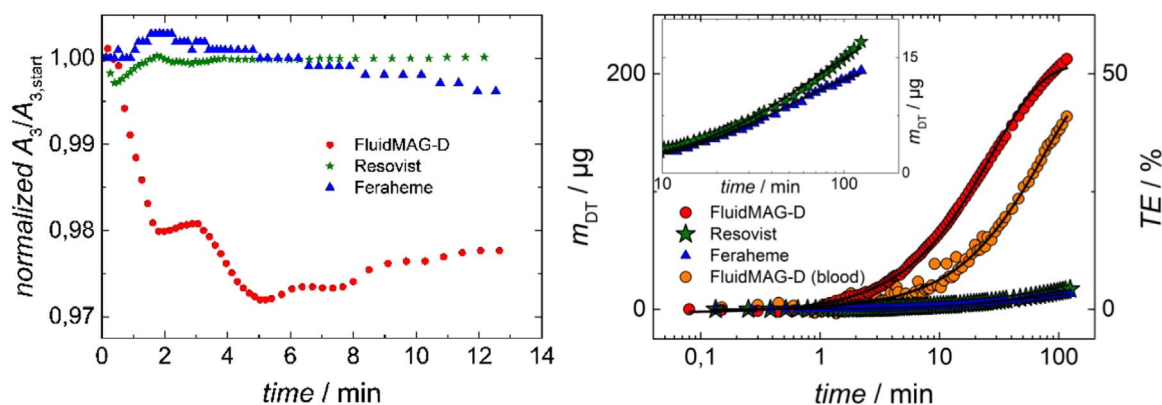
Fig. 4. Left: Transient behavior after filling the tube with the MNP suspension. After 15 min the deviation is below 1%. Right: Targeting efficiency of FluidMAG-D, Resovist, Feraheme suspended in water and FluidMAG-D suspended in blood. The initial total iron amount was 400 µg. Shown are the accumulated iron amounts in the retention area over a 120 min targeting interval together with fitted curves (black solid lines) according Eq. (7) to determine the maximum accumulated iron amount and the half-time period of each MNP type. The inset shows an enlarged view on the accumulated iron amounts of Resovist and Feraheme MNP.

FluidMAG-D it has been observed, that the amplitude A_3 after targeting (even 20 min circulating through the tube system) was significantly higher than at the beginning t_0 of the targeting experiment. Together with the observation that the slope of the MPS spectra (characterized by the shape factor A_5/A_3) also significantly changed (A_5/A_3 increased compared to the value at t_0) this was attributed to changes in the size distribution or in the magnetic interactions of the MNP (due to cluster formation) induced by the action of the targeting magnet. In the targeting using Feraheme and Resovist MNP this behavior could not be detected.

To describe the accumulated iron amount m_{DT} according to Eq. (6) as a function of time we used an exponential decay of first order

$$m_{DT}(t) = m_{max} \left(1 - \exp^{-t/\tau}\right) + m_0, \qquad (7)$$

with maximum accumulated amount m_{max} and time constant τ and an offset iron amount m_0. For practical purposes τ is translated into the half-life period $t_{1/2}$

$$t_{1/2} = \ln(2)\,\tau \qquad (8)$$

as the targeting time interval where half of the amount of m_{max} is retained. But, our half-life period $t_{1/2}$ must not be confused with the blood half-life of MNP due to clearance by liver and spleen.

3.4. The targeting efficiency of FluidMAG-D, Resovist and Feraheme MNP

In Fig. 4(right) targeting procedures for the three investigated MNP types FluidMAG-D, Resovist, and Feraheme suspended in water are shown. Additionally, a targeting experiment of FluidMAG-D MNP suspended in full blood is displayed. The straight (black) lines display the results of a curve fit according to Eq. (8) which was performed to determine the parameters m_{max} and $t_{1/2}$ (values are collected in Table 2).

The physical parameters flow rate (350 µL/min), targeting tube diameters (1.4 mm), magnetic field gradient (80 T/m) and total iron content in the tube system (around 400 µg) were kept identical for all passes. The targeting efficiency *TE* of Resovist and Feraheme of less than 5% is significantly smaller than for FluidMAG-D where *TE* amounts to over 50%. FluidMAG-D exhibited the shortest half-life period $t_{1/2}\sim18$ min whereas Resovist was only slowly enriched at the retention area ($t_{1/2}\sim47$ min). Interestingly, the targeting of FluidMAG-D suspended in blood has no considerable impact on *TE*, but leads to a half-life period more than twice the value observed in pure water. This demonstrates that MPS enables MNP quantification even in turbid solutions, thus providing direct access to important information about targeting efficiency of MNP in a physiological environment like blood.

3.5. Reproducibility of targeting measurements

To demonstrate the reproducibility of the targeting procedure using the flow phantom setup we repeated three targeting passes using FluidMAG-D at a concentration of 7.5 mmol/L and identical flow phantom system parameters (flow rate 350 µL/min, gradient 80 T/m, duration 120 min). From the targeting parameters of the fitted curves using Eqs. (7) and (8) a variation of the maximum accumulated MNP amount m_{max} of 6% and the half-life period $t_{1/2}$ of 9% were found for three consecutive measurements. These small deviations might be due to an upper concentration dependent limit of MNP which can be accumulated in the retention area. Another reason can be found in the positioning of the targeting magnet which was removed after each experiment and readjusted with an accuracy of 0.4 mm.

4. Conclusion

We established a tube flow phantom with incorporated MPS flow cell for quantification of the MDT efficiency of MNP. For three different MNP types we demonstrated that the tube flow phantom allows for studying in-vitro targeting of MNP under defined and controlled conditions and under influence of relevant physical and physiological MDT parameters. The major advantage of the flow phantom is the continuous quantification with a dedicated flow cell offering an outstanding detection limit of about one nanogram iron. In contrast to optical methods, the magnetic detection principle offers the possibility to study the MNP targeting efficiency even in turbid media as demonstrated for FluidMAG-D in full blood.

Furthermore, MPS can easily be deployed to test materials for magnetic contamination or adhesion of MNP. Accordingly, those side effects could be excluded for conducted experiments. Nevertheless, an MNP type dependent adhesion to the tubing material was observed. Therefore preliminary material tests are recommended.

The novel targeting phantom permits a highly accurate platform for the evaluation of the influence of various physiological and physical parameters in the complex application of magnetic targeting. The integration of an MPS device for the MNP specific detection permits the real-time contactless quantitative assessment of the targeting process. Moreover MPS is capable of detecting changes of MNP magnetism providing valuable information [16] which will be subject of future investigations.

Acknowledgements

No. TR 408/7-2).

References

[1] S. Goodwin, C. Peterson, C. Hoh, C. Bittner, Targeting and retention of magnetic targeted carriers (MTCs) enhancing intra-arterial chemotherapy, J. Magn. Magn. Mater. 194 (1–3) (1999) 132–139.

[2] C. Alexiou, W. Arnold, R.J. Klein, F.G. Parak, P. Hulin, C. Bergemann, Locoregional cancer treatment with magnetic drug targeting, Cancer Res. 60 (23) (2000) 6641–6648.

[3] A.S. Lübbe, C. Bergemann, W. Huhnt, T. Fricke, H. Riess, J.W., u.a. Brock, Preclinical experiences with magnetic drug targeting: tolerance and efficacy, Cancer Res. 56 (20) (1996) 4694–4701.

[4] A.S. Lübbe, C. Bergemann, H. Riess, F. Schriever, P. Reichardt, K., u.a. Possinger, Clinical experiences with magnetic drug targeting: a phase I study with 4′-epidoxorubicin in 14 patients with advanced solid tumors, Cancer Res. 56 (20) (1996) 4686–4693.

[5] B. Shapiro, S. Kulkarni, A. Nacev, S. Muro, P.Y. Stepanov, I.N. Weinberg, Open challenges in magnetic drug targeting: open challenges in magnetic drug targeting, Wiley Interdiscip. Rev.: Nanomed. Nanobiotechnol. 7 (3) (2015) 446–457.

[6] R. Jurgons, C. Seliger, A. Hilpert, L. Trahms, S. Odenbach, C. Alexiou, Drug loaded magnetic nanoparticles for cancer therapy, J. Phys: Condens Matter 18 (38) (2006) S2893.

[7] A. Lascialfari, In vivo biomedical applications of magnetic resonance and magnetic materials, La Riv. Nuovo Cim. 6 (2013) 211.

[8] P. Radon, M. Liebl, N. Pompner, M. Stapf, F. Wiekhorst, K., u.a. Gitter, Magnetic particle spectroscopy to determine the magnetic drug targeting efficiency of different magnetic nanoparticles in a flow phantom, IEEE Trans. Magn. 51 (2) (2015) 1–4.

[9] B. Gleich, J. Weizenecker, Tomographic imaging using the nonlinear response of magnetic particles, Nature 435 (7046) (2005) 1214–1217.

[10] S.R. Snyder, U. Heinen, Characterization of magnetic nanoparticles for therapy and diagnostics. Available online: ⟨https://www.bruker.com/fileadmin/user_upload/8-PDF-Docs/MagneticResonance/MRI/brochures/MPS_app-note.pdf⟩, 2010 (accessed on 14.05.16).

[11] N. Löwa, F. Wiekhorst, I. Gemeinhardt, M. Ebert, J. Schnorr, S., ua Wagner, Cellular uptake of magnetic nanoparticles quantified by magnetic particle spectroscopy, IEEE Trans. Magn. 49 (1) (2013) 275–278.

[12] A. Senyei, K. Widder, G. Czerlinski, Magnetic guidance of drug-carrying microspheres, J. Appl. Phys. 49 (6) (1978) 3578–3583.

[13] E.K. Ruuge, A.N. Rusetski, Magnetic fluids as drug carriers: targeted transport of drugs by a magnetic field, J. Magn. Magn. Mater. 122 (1–3) (1993) 335–339.

[14] M. Babincová, P. Babinec, C. Bergemann, High-gradient magnetic capture of ferrofluids: implications for drug targeting and tumor embolization, Z. Nat. C 56 (9–10) (2001) 909–911.

[15] S. Kayal, D. Bandyopathyay, T.K. Mandal, R.V. Ramanujan, The flow of magnetic nanoparticles in magnetic drug targeting, RSC Adv. 1 (2) (2011) 238.

[16] N. Löwa, P. Knappe, F. Wiekhorst, D. Eberbeck, A.F. Thünemann, L. Trahms, Hyphenation of field-flow fractionation and magnetic particle spectroscopy, Chromatography 2 (4) (2015) 655–668.

[17] E.P. Furlani, K.C. Ng, Nanoscale magnetic biotransport with application to magnetofection, Phys. Rev. E 77 (6) (2008) 061914-1–061914-8.

[18] D. Eberbeck, F. Wiekhorst, S. Wagner, L. Trahms, How the size distribution of magnetic nanoparticles determines their magnetic particle imaging performance, Appl. Phys. Lett. 98 (18) (2011) 182502-1–182502-3.